analytical chemistry

Article

Cite This: Anal. Chem. 2018, 90, 10271−10278

pubs.acs.org/ac

Impact of the Particle Diameter on Ion Cloud Formation from Gold Nanoparticles in ICPMS

Joshua Fuchs,[†] Maryam Aghaei,[‡] Tilo D. Schachel,[†] Michael Sperling,[†,§] Annemie Bogaerts,*[,‡] and Uwe Karst*[,†]

[†]Institute of Inorganic and Analytical Chemistry, University of Münster, Corrensstrasse 28/30, 48149 Münster, Germany

[‡]Research Group PLASMANT, Chemistry Department, University of Antwerp, Universiteitsplein 1, 2610 Antwerp, Belgium

[§]European Virtual Institute for Speciation Analysis, Mendelstrasse 11, 48149 Münster, Germany

Supporting Information

ABSTRACT: The unique capabilities of microsecond dwell time (DT) single-particle inductively coupled plasma mass spectrometry (spICPMS) were utilized to characterize the cloud of ions generated from the introduction of suspensions of gold nanoparticles (AuNPs) into the plasma. A set of narrowly distributed particles with diameters ranging from 15.4 to 100.1 nm was synthesized and characterized according to established protocols. Statistically significant numbers of the short transient spICPMS events were evaluated by using 50 μs DT for their summed intensity, maximum intensity, and duration, of which all three were found to depend on the particle diameter. The summed intensity increases from 10 to 1661 counts and the maximum intensity from 6 to 309 counts for AuNPs with diameters from 15.4 to 83.2 nm. The event duration rises from 322 to 1007 μs upon increasing AuNP diameter. These numbers represent a comprehensive set of key data points of the ion clouds generated in ICPMS from AuNPs. The extension of event duration is of high interest to appoint the maximum possible particle number concentration at which separation of consecutive events in spICPMS can still be achieved. Moreover, the combined evaluation of all above-mentioned ion cloud characteristics can explain the regularly observed prolonged single-particle events. The transport and ionization behavior of AuNPs in the ICP was also computationally modeled to gain insight into the size-dependent signal generation. The simulated data reveals that the plasma temperature, and therefore the point of ionization of the particles, is the same for all diameters. However, the maximum number density of Au^+, as well as the extent of the ion cloud, depends on the particle diameter, in agreement with the experimental data, and it provides an adequate explanation for the observed ion cloud characteristics.

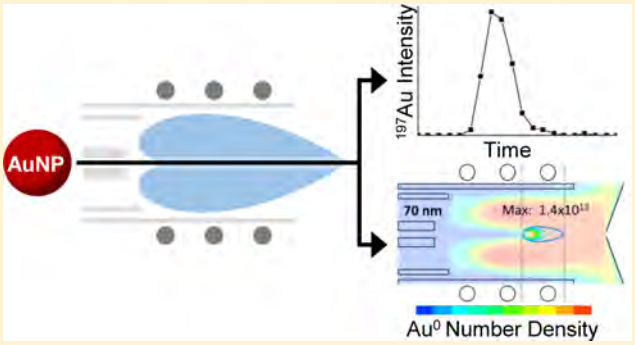

Engineered nanomaterials (ENMs), a major product of the rapid development of nanotechnology over the last couple of decades, have attracted great interest in the field of analytical chemistry. By now, numerous ENMs are used in consumer products of daily life, yet also in medical applications and treatments, which leads to significant release into the environment.[1−4] Addressing the fate and risk assessment calls for extensive and reliable analytical methods capable of rapid analysis of ENMs from complex matrixes.[5] Several techniques for ENM characterization are readily available. Electron microscopy is probably the most powerful technique for extensive ENM analysis but requires sophisticated sample preparation.[6,7] Other methods, such as light scattering or UV−vis absorption spectroscopy, have a look at the whole particle ensemble in solution and not at the specific single particle itself.[8,9] Anyway, to gain comprehensive information on all different ENM characteristics, multiple techniques have to be utilized or specific methods need to be applied for answering a particular question. An emerging technique for the analysis of metallic or oxide nanoparticles is inductively coupled plasma mass spectrometry operated in single-particle mode (spICPMS).[10]

Since the introduction of the ICP as an ion source for mass spectrometry in 1980,[11] it has emerged as one of the most used and accepted analytical techniques for trace element analysis.[12] Although ICP optical emission spectroscopy was used to investigate airborne particles in sufficiently low concentrations already in the 1980s,[13−15] only in 2003 did Degueldre and co-workers adapt it for the analysis of inorganic colloids, such as rutile, alumina, and gold, from highly diluted aqueous suspension by ICPMS.[16−19] Since then, the possibility of spICPMS for the analysis of ENMs was presented in numerous publications. Among others are the analysis of nanoparticles from suspensions besides ionic species of the element of interest, the utilization in immunoassay strategies, in experi-

Received: May 4, 2018
Accepted: July 30, 2018
Published: July 30, 2018

DOI: 10.1021/acs.analchem.8b02007
Anal. Chem. 2018, 90, 10271−10278

ments to investigate particle diameters compared to other methods, or to determine transport efficiencies into an ICP.[20−23] Anyway, for further development of the methodology, the processes leading to the signal generation must be fully understood. Already back in 1992, Hobbs and Olesik observed large fluctuations in the ICPMS signal on the microsecond time scale and related them to incomplete vaporization of particles in the plasma.[24] Olesik's group obtained further insight into signal and ion cloud formation in the ICP by time-resolved mass spectrometry and optical emission spectroscopy. They observed the width of a Li^+ ion cloud expanding to a duration of 272 μs at 10 mm after vaporization, when introduced by a monodisperse dried microparticulate injector (MDMI).[25,26] Aeschliman et al. studied the fate of dried solution aerosols and solid particles with high-speed photography.[27] All this work led to an improved understanding of signal generation in ICP techniques. However, to acquire and handle these short transient signals remained a challenging topic, yet it opens up new applications in ICPMS-based research.[28] By enhancing the rate of data acquisition in spICPMS, the ion cloud produced from solely introduced nanoparticles can be temporally resolved and further studied.[29] A shorter acquisition time is already used in the latest studies, as it facilitates the differentiation of signals produced from nanoparticles or ionic background species and improves particle counting rates.[30−33]

Since the beginning of fundamental plasma research, computer modeling has shown to be a powerful tool to study the plasma characteristics. A brief overview of computational investigations from literature can be found in the tutorial paper of Bogaerts and Aghaei.[34] Furthermore, the PLASMANT group (plasma, laser ablation and surface modelling—Antwerp) developed a computational model that describes the plasma characteristics, gas flow patterns, sample transport, evaporation, and ionization relevant for analytical purposes. The model was already successfully used to optimize plasma conditions, to describe the influence of a mass spectrometer interface, and to study the fate of copper particles introduced into an ICP.[35−42]

In this study, fast data acquisition times of 50 μs of a commercially available instrument are used to study the ion cloud formation of gold nanoparticles (AuNPs) in a comprehensive way, by introducing a set of narrowly distributed AuNPs with intentionally tuned mean diameters. The recorded data is evaluated thoroughly and at statistically relevant levels. Furthermore, to better understand the signal generation from AuNPs in spICPMS, the transport of the nanoparticles in the ICP, as well as their vaporization and ionization, are simulated by a computational model and compared to the experimental data. This comparison gives insight into the fundamental AuNP ion cloud characteristics and provides crucial information, supporting further spICPMS method development by ascertaining a set of reliable figures of the ion cloud characteristics. These numbers will aid to evaluate whether events in spICPMS are originating from the introduction of single particles or from artifacts, e.g., the introduction of particle aggregates or double-particle events. This will help to elucidate maximum applicable particle number concentrations and minimal required dwell time (DT) in spICPMS. Instrument parameters chosen match those commonly utilized in spICPMS analysis, and thus the obtained figures can be used as indicators for the same kind of study on other instruments, which will help to make the acquired data more reliable and provide starting points for system diagnosis, which will help to improve detection capabilities in spICPMS.

EXPERIMENTAL SECTION

Chemicals. Commercially available AuNP suspensions with diameters of 15.4 (±1.0), 20.0 (±2.5), 31.0 (±3.3), 40.3 (±3.3), 48.2 (±6.6), and 60.8 (±7.0) nm were purchased from NanoComposix (San Diego, U.S.A.). These nanoparticle suspensions were used as references for characterization of self-synthesized AuNP and as samples for the ion cloud study. Gold(III) chloride trihydrate ($HAuCl_4$, >99.9%) and trisodium citrate dihydrate (SC, >99.5%) were purchased from Sigma-Aldrich. Double-distilled water (ddH_2O) was obtained using a water still Aquatron A4000D (Bibby Scientific, Stone, U.K.).

AuNP Synthesis and Characterization. AuNPs with narrow size distributions and different diameters between 16.4 and 100.1 nm were synthesized according to the seeded-growth protocol of Bastús et al.[43] The AuNPs were characterized by UV−vis absorption and transmission electron microscopy (TEM). For detailed information on the synthesis and the characterization, we refer to the Supporting Information.

spICPMS Analysis. All ICPMS data in this work was acquired using a AnalytikJena PlasmaQuant MS Elite quadrupole-based plasma mass spectrometer (Jena, Germany) in time-resolved-analysis (TRA) mode either with a DT of 10 ms to capture the whole particle event all at once or 50 μs to gain insight into the profile of the formed ion cloud. Samples were sonicated for 1 min and subsequently diluted with ddH_2O to a number concentration suitable for spICPMS analysis. The ICP instrument was tuned for optimal ^{197}Au sensitivity. All used instrument and spICPMS parameters are listed in Table S-1.

Single-particle events of each suspension were plotted as cubic root intensity histograms, the distribution of the intensities was fitted with a Gaussian function using OriginPro 2016G software. The mean intensity was plotted against particle diameter obtained by TEM analysis to ensure overall linearity of the instrument throughout the whole particle batch.

A microsecond DT of 50 μs was used to obtain information on the temporal profile of the ion cloud generated by a single particle entering the plasma. Readout and settling of the detector required 35 μs, thus resulting in a data point acquired every 85 μs. All particle suspensions were introduced for a total time of 300 s, but were split into 10 subsequent measurements of 10 s each, repeated twice, in order to allow for the safe storage of the large amount of data points at those short dwell times. To handle the data post analysis, a self-written Java application was utilized to identify start and end of the single-particle events. The total summed intensity, maximum intensity, and event duration were calculated from this data.

Computational Model. A comprehensive self-written fluid dynamics model was developed within the commercial computational fluid dynamics (CFD) program FLUENT 16.0.0 (ANSYS). This model describes the gas flow dynamics, plasma behavior, and sample introduction in the ICP torch, considering the large pressure drop from upstream to downstream (i.e., 1 atm to 1 Torr) of the mass spectrometer interface.[37,38] In this model, the transport parameters of the species were for the first time calculated self-consistently for the gas mixture under study. Therefore, it is possible to apply this model to different gas mixtures, e.g., a mixture of gold and argon in this study. Details about this model can be found in

DOI: 10.1021/acs.analchem.8b02007
Anal. Chem. 2018, 90, 10271−10278

Table 1. Nominal Notation and Diameter (±SD) Obtained from TEM Analysis for All Used AuNPs, as Well as the Determined Ion Cloud Characteristics: Summed Intensity, Maximum Intensity, and Event Duration

AuNP nos.	D_{TEM} (±SD) /nm	summed intensity /counts	max intensity /counts	duration /μs
15	15.4 (1.0)	10.4		322
16	16.4 (1.3)	13.0		384
20	20.0 (2.5)	20.8	5.8	471
25	24.6 (1.9)	44.3	10.8	590
31	31.0 (3.3)	89.3	21.3	684
37	36.8 (3.0)	150.4	35.7	734
40	40.3 (3.3)	210.2	45.8	779
48	48.2 (6.6)	327.1	71.5	834
54	54.2 (3.7)	395.6	90.7	836
60	60.8 (7.0)	645.0	134.2	906
71	71.3 (5.5)	1084.5	221.9	955
83	83.2 (6.7)	1661.1	308.6	1007
100	100.1 (6.8)		493.2	

refs 36 and 41. Details on the most relevant part of the model for the present study, i.e., the so-called "discrete phase model" (DPM) to describe the sample transport in the ICP, can be found in the Supporting Information.[44−46]

RESULTS

Particle Characterization. Nanoparticle synthesis following the seeded-growth protocol of Bastús et al. yielded suspensions of wine-red gold NPs. UV−vis absorption spectra are shown in Figure S-1. Symmetrical absorption and a shift of the absorption maxima from 520 to 560 nm is observed for all particle suspensions, which indicates monodisperse particle distributions and increasing particle diameters, respectively. All spectra are normalized at 400 nm. Figure S-2 shows TEM images for all synthesized NPs. The diameter increases with each growth step, and a spherical geometry was achieved. Particle diameters were calculated from at least 100 particles to be 16.4 (±1.3), 24.6 (±1.9), 36.8 (±3.0), 54.2 (±3.7), 71.3 (±5.5), 83.2 (±6.7), and 100.1 (±6.8) nm (Table 1). The particle suspensions are further named for their nominal size, e.g., AuNP16. These particle suspensions exhibit overall narrow size distributions and complement the ones commercially obtained, which allows us to monitor small changes in ion cloud characteristics. To ensure complete collection of the ion clouds, and therefore linearity of the ICP response, all particle suspensions were analyzed in spICPMS mode using 10 ms DT. The intensity of single-particle events from the raw TRA signal was plotted as histograms using the cubic root of intensity, to take the relation between particle mass, volume, and diameter into account, thus allowing the fitting of Gaussian functions. Cubic roots of mean for all Gaussian fits from all suspensions, commercial as well as synthesized, were plotted versus particle diameter obtained by our own or the manufacturer's TEM analysis accompanied by error bars, indicating one standard deviation of either spICPMS data or TEM data (Figure S-4). The error bars of the synthesized particles were found to be smaller in general. A linear fit revealed a calibration function with a correlation coefficient of 0.999 for particles from 15.4 to 83.2 nm taking both particle sets into account, which confirms complete ionization and linear response for the cubic root of the ICP intensity. The mean intensity for AuNPs with a diameter of 100.1 nm was found to be lower than expected from extrapolation of the calibration curve, which indicates that these particles are not completely ionized anymore using the applied plasma conditions; thus, particles greater than 83.2 nm would be underestimated in mass and therefore size.

Microsecond Data Acquisition and Evaluation. All consecutive measurements of one NP suspension over the total of 300 s at 50 μs DT add up to roughly 3.5 million data points, containing around 2500 single-particle events, not taking background noise into account. For all 85 μs, the number of ions counted in a period of one 50 μs DT was recorded. The general shape of the ion clouds produced from one single-particle event exhibits a steep increase at the beginning, followed by a maximum and a less steep slope for later time and flattening in the end. Previously reported durations of single-particle events are stated of being around half a millisecond and seemed to be not significantly influenced by the material of the particle or the spectrometer. Nonetheless, the number of evaluated single-particle events was held small and the influence of the particle diameter was not considered.[31,47] This study focuses on the impact of the diameter on the duration of these short transient signals with statistically relevant numbers of events.

To transform the raw data into frequency distributions for all events, both particles and background, an algorithm-based evaluation needs to be applied. A self-written Java application was utilized. It scanned the whole TRA signal for the start of a single-particle event, which could be achieved in a straightforward way by using each data point above zero counts as starting point, because of the virtual absent background for gold at this low DT. After identifying the start, all following counts were summed to give the total summed intensity per particle event, until the signal reached zero counts again, marking the end of an event. The signal duration was determined by multiplying the number of data points obtained for an event with 85.2 μs, which was found to be the average time between two integration intervals. The highest occurring signal was taken as the maximal intensity of each event. This approach resulted in three features per single-particle event, namely, the summed intensity, maximum intensity, and signal duration. All obtained features were transferred into frequency distributions. Gaussian functions were fitted, if possible, and mean values were plotted versus particle diameter. An overview of the fitted Gaussian functions and the influence of particle diameter on these frequency distributions for three AuNPs of different size is shown in Figure 1 (maximum intensity and signal duration) and Figure S-3 (summed intensity) and will be

DOI: 10.1021/acs.analchem.8b02007
Anal. Chem. 2018, 90, 10271−10278

discussed in detail in the next section and in the Supporting Information, respectively.

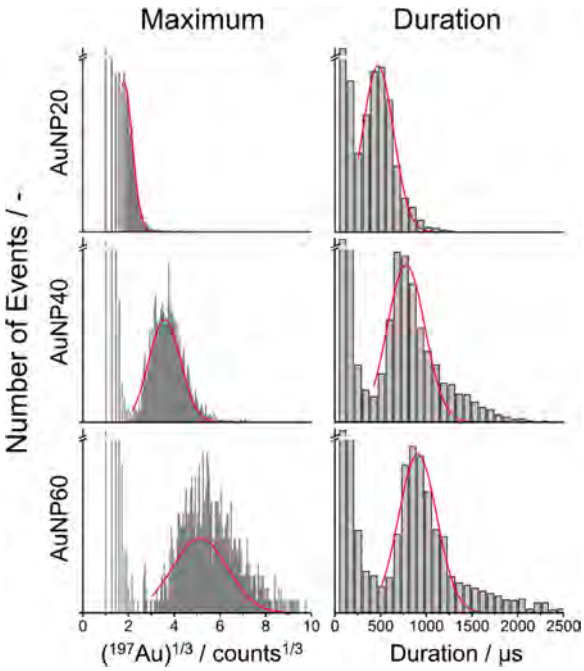

Figure 1. Frequency distributions of maximum intensity and event duration obtained for three different sizes of AuNPs as example. Data of maximum intensity is plotted as the cubic root to account for the cubic relation of particle volume or mass and diameter allowing us to apply a linear Gaussian fit (red line). The left-sided, not-fitted bars are contributions of the background noise. All horizontal axes share the same scale in one column.

Total Summed Intensity of Single-Particle Events. As described in the previous section, all single-particle events of each suspension were evaluated for their total summed single-particle event intensity to ensure linearity of the detector response over the course of all introduced particle sizes using 50 μs DT. The influence of particle diameter on the summed signal intensity can be seen in Figure S-3, where the frequency distributions for AuNP20, 40, and 60 are depicted as an example as well as means of Gaussian fit obtained from the frequency distributions of each particle suspension versus the particle diameter. The information gained from the summed signal intensity at microsecond DT is merely the same as at millisecond DT, but nonetheless, the use of microsecond DT is a suitable tool to minimize background counts from ionic species present in the sample and ultimately enables the study of ion cloud characteristics of single-particle events entering the plasma.[30]

Maximum Intensity of Single-Particle Events. Evaluation of the maximum signal intensity per single-particle event for each particle suspension exhibits a similar behavior as for the summed intensity (Figure S-3). In the left column of Figure 1, the distributions of the maximum intensities of the events are depicted. All three different particle sizes share the same horizontal axes. The distribution of maximum intensity for AuNP20 can only be recognized as a shoulder emerging from the background noise, yet an estimate of the mean can be obtained as shown by the indicated fit. However, no distribution could be obtained for AuNP suspension smaller 20 nm. The mean of the distribution is moving toward higher counts with increasing particle size. For the largest AuNP suspensions, distributions of the maximum intensity were obtained and no secondary distribution emerged. All means designated from fitting Gaussian functions were plotted versus particle diameter obtained by TEM analysis, either fitted linearly for cubed root values or using a three-degree polynomial with correlation coefficients of 0.999 and 0.996, respectively (Figure 2A), hence exhibiting the same trend as

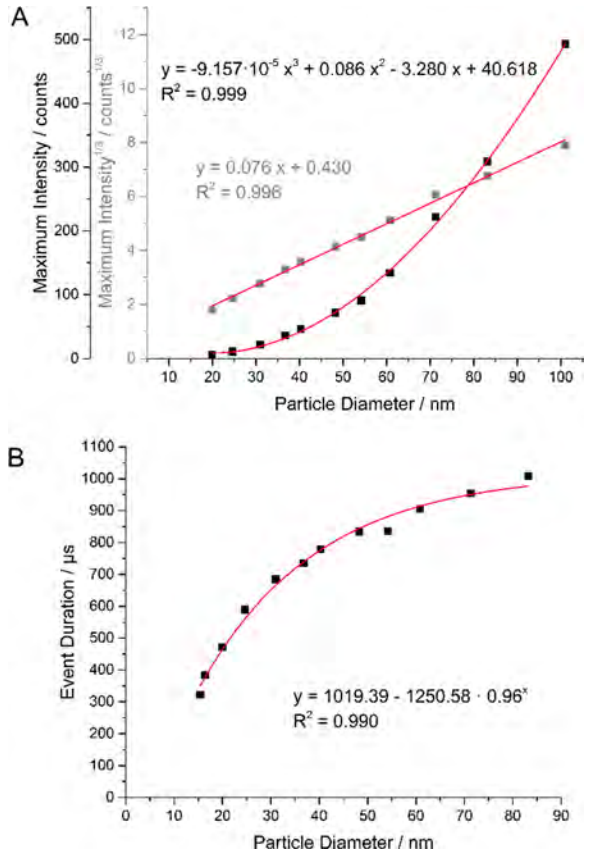

Figure 2. Means of Gaussian fit obtained from the frequency distributions of each particle suspension for the maximum intensity (A) and event duration (B) vs particle diameter as obtained from TEM analysis. In panel A, the cubic root of maximum intensity is also plotted (gray data points and gray *y*-axes), showing a linear relationship with particle diameter, thus confirming the cubic relationship of particle volume or mass vs particle diameter.

seen for the summed intensity. The overall number of counts found at the maximum of single-particle events is lower than the total summed intensity, which is consistent, as at the maximum only a portion of the complete ion cloud is captured at the detector. The means of maximum intensity range from 5.8 to 493.2 counts for AuNP20–AuNP100, respectively.

Event Duration of Single-Particle Events. The frequency distributions of single-particle event duration for AuNP20, 40, and 60 are also shown in Figure 1 (right column). The axes are again kept in the same scale for all three sizes. The most pronounced event duration shifts toward longer duration with increasing particle diameter, similar to the summed and maximum intensity. A large portion of AuNP20 distribution overlaps with the background events. Even the distribution obtained for AuNP60 is not fully separated from the background. Prolonged particle event durations above 1250 μs are observed for larger AuNPs, which will be discussed

DOI: 10.1021/acs.analchem.8b02007
Anal. Chem. 2018, 90, 10271−10278

in the following section. Gaussian functions were fitted, to get an average single-particle event duration, albeit ignoring the prolonged durations observed for larger particles. The mean values obtained in this way are plotted in Figure 2B versus particle diameters. For the smallest particles, AuNP15, the mean event duration is found to be 322 μs, while it rises to 924 μs for AuNP83. Like what was observed for the summed intensity, the histograms of the event duration exhibit two distributions for particle sizes above 71.3 nm: one in a range of durations that is expected by extrapolating from particles with smaller diameters, and one with far too short durations in the range of AuNP20. These artifacts can be assigned to particle events not completely recorded, as also observed for the summed intensity. In fact, if both the information on summed intensity and duration is taken into account, too few counts in summed intensity correlates to too short duration for those events. Yet, if the second distribution is evaluated, meaningful results can be obtained. A nonlinear behavior is observed as the change in particle duration is found to be less for larger particle diameters than for smaller particles. An asymptotic exponential fit can be applied, which provides a regression coefficient of 0.990 and tends toward 1019 μs as maximum.

Prolonged Particle Events. The observed prolonged single-particle events for larger AuNPs are of special interest. Since for each single-particle event all three characteristics, i.e., summed intensity, maximum, and duration, besides the ion cloud profile itself, are obtained, a more detailed picture of these events can be obtained. A visualization for AuNP40 is shown in Figure 3, and should function as an example of this approach. The upper section compares all single-particle events of AuNP40 for their event duration (horizontal axis) with their summed intensity (vertical axis). The summed intensity data is plotted as cubic root. Each marker represents one single-particle event, and all are displayed partially transparent so that areas of most frequent values occur darker, whereas less frequent values exhibit a gray shade. For clarification, the previously obtained frequency distributions of event duration and summed intensity, with overlaid, fitted Gaussian functions, are shown at the edges of this 2D plot. It can be seen that darker areas of more frequent values correlate to the means of the distributions. The lower section connects maximum intensity with event duration in the same manner as described for summed intensity and duration. All events found in the lower left corner of each 2D plot contribute to the background noise, which is clearly separated from the single-particle events by all three characteristics.

The mentioned prolonged particle events are occurring at event durations above roughly 1250 μs. Checking the upper 2D plot, it can be seen that, even though the particle duration is prolonged, the total summed intensities per event are spread all over the distribution. This means that they do not arise from particularly large particles but are found randomly for all statistically distributed particle diameters of a monodisperse NP suspension. This is not the case for the maximum intensity, as can be seen in the lower section of Figure 3. The prolonged particle events share their maximum intensity on the flank of lower values of the distribution. The decrease of the maximum intensity is even more present for longer durations, leading to an overall curvy shape in the 2D plot. This behavior is found for all particle sizes and leads to the conclusion that prolonged particle events are caused by normally large particles, which travel more slowly through the plasma and therefore experience more diffusion and widening of the ion cloud.

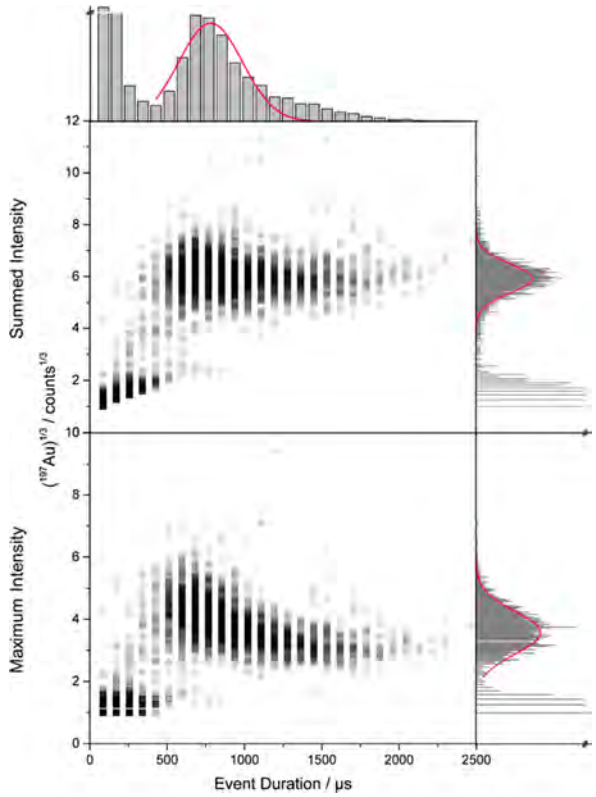

Figure 3. Two-dimensional visualization of all three single-particle event characteristics for AuNP40. Each square represents one single-particle event and is placed in the 2D plot either for its summed intensity and event duration (upper section) or maximum intensity and event duration (lower section). The squares are plotted in a transparent way so that areas of more frequent event characteristics appear darker, which is also indicated by the histograms of summed and maximum intensity (vertical axes) and event duration (horizontal axis).

Indeed, this causes the detection of the same summed intensity, but over a longer course with less high signal intensities.

Au^+ Number Density. Computer simulations can provide information on characteristic features of an ICP, including the number density of Au^+ ions inside the plasma torch.[34] The calculated number density is compared to the experimental data obtained by spICPMS to check if Au^+ generation from AuNP of different diameters matches the experiments and simulations. If so, the simulated plasma parameters can further be used to provide adequate explanations for the observed ion cloud characteristics. Therefore, eight different particle sizes were simulated, ranging from 20 to 70 nm in diameter. The operating conditions were kept close to the experiments, which are shown in Table S-1. Note that the operating parameters, such as plasma power, sample and gas flow rates, as well as geometrical conditions, also affect the particle ionization behavior, as shown by Bogaerts and Aghaei for copper particles, as a case study, in the ICP torch.[34] Two-dimensional axisymmetric profiles of the calculated Au^+ number density are shown in Figure 4. The overall number density rises and expands along the central axis, as well as in the radial direction, with increasing particle diameter. Notably, the area of maximum ion density is found at the same point along the central axis, which coincides with the maximum plasma temperature along the central axis. Since the operating

DOI: 10.1021/acs.analchem.8b02007
Anal. Chem. 2018, 90, 10271−10278

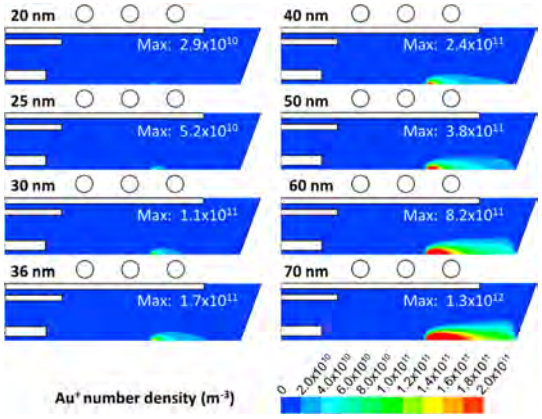

Figure 4. Two-dimensional profiles of Au^+ number density for AuNPs of different diameters. The maximum densities (in m^{-3}) are also indicated. Only half of the 2D axisymmetric torch is plotted.

parameters (e.g., rf power, Ar gas flow rates, etc.) and geometrical conditions for all the cases were kept the same, the position of maximum plasma temperature stays the same. It is shown in ref 34 that, for a particle loading rate up to 1 μg/s, the effect on the plasma temperature is minor. Therefore, in the current study, where the particle loading rate varies from 0.6 to 27 fg s^{-1} for particle diameters of 20−70 nm, the temperature profile stays undisturbed (see Figure 6). For all particle diameters the highest number density is reached well before the sampler orifice. To underline this, the number density of Au^+ ions along the central axis is shown in Figure S-6. Ionization begins between the second and third winding of the coil, where the plasma temperature typically reaches levels of the boiling point for gold of 3080 °C.[38,48] All particles exhibit a similar shape of Au^+ number density. A steep increase, followed by a sharp maximum at the same position, is observed for all diameters. The density drops afterward, but remains constant until reaching the sampler position. However, the number density of Au^+ stays at higher levels over a longer time downstream the central axis for larger particles. Figure S-7 depicts the radial number density profile right at the sampler position. It is the highest right in front of the sampler orifice, with the absolute maximum in the center position and decreasing toward the edges. The sharp minimum at about 0.5 mm from the orifice center is due to the cooling effect of the sampler, which has an orifice of 1 mm diameter.[37] The maximum Au^+ number density is increasing with particle diameter at the sampler position, which is leading to a larger number of ions being extracted into the mass analyzer and eventually a higher detected signal. The maximum and average number density of Au^+ along the central axis as well as at the sampler orifice are plotted versus particle diameter in Figure 5. The number density in all cases clearly follows the same cubic trend as observed from the experimental data, and thus it explains the increase in ^{197}Au ion counts in spICPMS analysis.

Au^0 Number Density. Two-dimensional profiles of the Au^0 number density as well as plasma temperature were also computed (Figure 6). All profiles are plotted in the same scale.

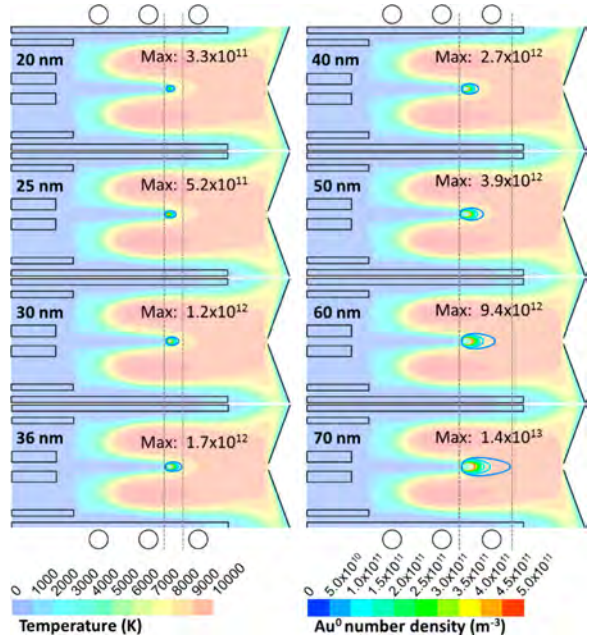

Figure 6. Two-dimensional profiles of atomic Au number density for AuNPs of different diameters. The maximum densities (in m^{-3}) are also indicated. For comparison, the plasma temperature contour lines are also plotted in faint colors, showing that the temperature profile is not affected by the NP introduction. The vertical dashed lines indicate the atomic cloud length for the AuNPs of 36 nm (left panels) and 70 nm (right panels), indicating that the atomic cloud extends over a wider region for the larger NPs.

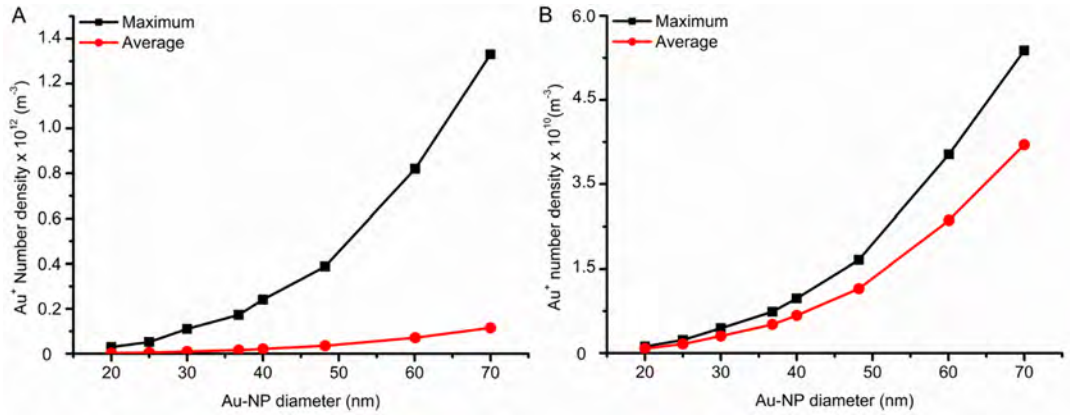

Figure 5. Maximum (black) and average (red) Au^+ number density calculated along the central axis (A) and at the sampler orifice (B), as a function of AuNP diameter.

DOI: 10.1021/acs.analchem.8b02007
Anal. Chem. 2018, 90, 10271−10278

As mentioned above, at the size and loading rate of the NPs in this study, the plasma temperature was found to be undisturbed. The formation of the atomic cloud starts at the end of the cool central inlet channel, when the temperatures of the plasma gas reaches the vaporization point of gold, regardless of the particle size. Nonetheless, the extent of the atomic cloud grows with increasing particle diameter, which is indicated by the dashed vertical lines, demarking start and end of the atomic cloud for AuNP36 (left column) and AuNP70 (right column). Thus, it takes longer for larger particles to get completely atomized and eventually ionized, providing a longer lasting source of ions, which ends closer to the sampler. This leads to a larger extended ion cloud, signal intensity, and event duration. The same is observed in the experimental data, where the maximum intensity and duration of the single-particle events increase for larger NPs.

CONCLUSION

A set of 13 narrowly distributed citrate-capped AuNPs with well-defined diameters from 15.4 to 100.1 nm were synthesized and successfully characterized by established methods for NP analysis as well as spICPMS with millisecond dwell time. Algorithm assistance allowed comprehensive and statistical relevant evaluation to appoint reliable figures for the three studied ion cloud characteristics, whereas all measurements were performed using established spICPMS operational parameters reported in literature with a commercially available quadrupole-based instrument.

This data shows that the duration of single-particle events is heavily influenced by the particle diameter, increasing the duration of these short transient signals from 322 μs for AuNP15 to 1007 μs for AuNP83. It demonstrates how important it is to extensively evaluate and correct data for split-particle events when using DTs in the range of 1 ms and especially if spICPMS is used for determination of particle number concentrations. Nonetheless, the influence of other experimental parameters, such as plasma power, gas flow rates, or sample matrix should be considered in further experiments, as they probably will have influence on the ion cloud formation.

A 2D axisymmetric model allowed us to qualitatively explain the characteristics of the observed ion clouds. It confirmed that the total summed single-particle signal intensity and maximum signal intensity increase with particle diameter on a cubic basis. The plasma temperature profile is undisturbed by the introduction of the AuNPs at this loading rates. This causes the ionization of the NPs to start all at the same point downstream the plasma. As the total time which the particles need to be atomized completely increases with particle size, it also permits the ion cloud to expand further, and eventually it increases the event duration as a function of particle diameter. This indicates that the calibration of spICPMS systems for size determination purpose should be done with nanoparticles of known size, rather than ionic standards, which probably will exhibit different ionization behavior in the plasma. The agreement of simulated and experimental results opens up possibilities for further study of the phenomena in spICPMS and influence of instrument parameters by the combination of both approaches.

The application of multimodal analysis on substantially prolonged single-particle event artifacts revealed that those do not emerge from particularly larger particles, aggregates, or multiparticle events. Prolonged events exhibit the same total summed intensities as normally short events but possess only one less pronounced maximum. This can be traced back to single particles traveling more slowly through the plasma. Thus, it illustrates the beneficial effect of monitoring all three characteristics of the ion cloud to enhance the certainty of NP analysis by spICPMS.

ASSOCIATED CONTENT

Supporting Information

The Supporting Information is available free of charge on the ACS Publications website at DOI: 10.1021/acs.analchem.8b02007.

Particle synthesis and characterization, computational model, total summed intensity of single-particle events, UV−vis spectra, TEM images, frequency distributions of summed intensity, mean intensity of single-particle events vs particle diameter, visualization of occurring secondary distribution, Au^+ number densities, and spICPMS operational parameters (PDF)

AUTHOR INFORMATION

Corresponding Authors

*E-mail: annemie.bogaerts@uantwerpen.be.
*E-mail: uk@uni-muenster.de. Phone: +49-251-83-33141.

ORCID

Maryam Aghaei: 0000-0003-4995-8773
Annemie Bogaerts: 0000-0001-9875-6460
Uwe Karst: 0000-0002-1774-6787

Notes

The authors declare no competing financial interest.

ACKNOWLEDGMENTS

We thank Dr. Harald Rösner from the Institute of Materials Physics of the University of Münster for the TEM imaging.

REFERENCES

(1) Vance, M. E.; Kuiken, T.; Vejerano, E. P.; McGinnis, S. P.; Hochella, M. F.; Rejeski, D.; Hull, D. R. *Beilstein J. Nanotechnol.* **2015**, *6* (1), 1769−1780.
(2) Wagner, V.; Dullaart, A.; Bock, A.-K.; Zweck, A. *Nat. Biotechnol.* **2006**, *24* (10), 1211−1217.
(3) Dreaden, E. C.; Alkilany, A. M.; Huang, X.; Murphy, C. J.; El-Sayed, M. A. *Chem. Soc. Rev.* **2012**, *41* (7), 2740−2779.
(4) Gottschalk, F.; Nowack, B. *J. Environ. Monit.* **2011**, *13* (5), 1145−1155.
(5) Alvarez, P. J. J.; Colvin, V.; Lead, J.; Stone, V. *ACS Nano* **2009**, *3* (7), 1616−1619.
(6) Wang, Z. L. *J. Phys. Chem. B* **2000**, *104* (6), 1153−1175.
(7) Mavrodcordatos, D.; Perret, D.; Leppard, G. G. In *Environmental Colloids and Particles: Behaviour, Separation and Characterisation*; Wilkinson, K. J., Lead, J. R., Eds.; John Wiley & Sons, Ltd.: Chichester, U.K., 2007; pp 345−391.
(8) Murdock, R. C.; Braydich-Stolle, L.; Schrand, A. M.; Schlager, J. J.; Hussain, S. M. *Toxicol. Sci.* **2008**, *101* (2), 239−253.
(9) Willets, K. A.; Van Duyne, R. P. *Annu. Rev. Phys. Chem.* **2007**, *58* (1), 267−297.
(10) Montaño, M. D.; Olesik, J. W.; Barber, A. G.; Challis, K.; Ranville, J. F. *Anal. Bioanal. Chem.* **2016**, *408* (19), 5053−5074.
(11) Houk, R. S.; Fassel, V. A.; Flesch, G. D.; Svec, H. J.; Gray, A. L.; Taylor, C. E. *Anal. Chem.* **1980**, *52* (14), 2283−2289.
(12) Montaser, A. *Inductively Coupled Plasma Mass Spectrometry*, 3rd ed.; Montaser, A., Ed.; Wiley-VCH: New York, 1998.
(13) Kawaguchi, H.; Fukasawa, N.; Mizuike, A. *Spectrochim. Acta, Part B* **1986**, *41* (12), 1277−1286.

DOI: 10.1021/acs.analchem.8b02007
Anal. Chem. 2018, 90, 10271−10278

(14) Bochert, U. K.; Dannecker, W. *J. Aerosol Sci.* **1989**, *20* (8), 1525−1528.
(15) Bochert, U. K.; Dannecker, W. *J. Aerosol Sci.* **1992**, *23*, 417−420.
(16) Degueldre, C.; Favarger, P. Y. *Colloids Surf., A* **2003**, *217* (1−3), 137−142.
(17) Degueldre, C.; Favarger, P. Y. *Talanta* **2004**, *62* (5), 1051−1054.
(18) Degueldre, C.; Favarger, P. Y.; Bitea, C. *Anal. Chim. Acta* **2004**, *518* (1−2), 137−142.
(19) Degueldre, C.; Favarger, P.-Y.; Wold, S. *Anal. Chim. Acta* **2006**, *555* (2), 263−268.
(20) Laborda, F.; Jiménez-Lamana, J.; Bolea, E.; Castillo, J. R. *J. Anal. At. Spectrom.* **2011**, *26* (7), 1362.
(21) Hu, S.; Liu, R.; Zhang, S.; Huang, Z.; Xing, Z.; Zhang, X. *J. Am. Soc. Mass Spectrom.* **2009**, *20* (6), 1096−1103.
(22) Pace, H. E.; Rogers, N. J.; Jarolimek, C.; Coleman, V. a; Gray, E. P.; Higgins, C. P.; Ranville, J. F. *Environ. Sci. Technol.* **2012**, *46* (22), 12272−12280.
(23) Pace, H. E.; Rogers, N. J.; Jarolimek, C.; Coleman, V. A.; Higgins, C. P.; Ranville, J. F. *Anal. Chem.* **2012**, *84* (10), 4633−4633.
(24) Hobbs, S. E.; Olesik, J. W. *Anal. Chem.* **1992**, *64* (3), 274−283.
(25) French, J. B.; Etkin, B.; Jong, R. *Anal. Chem.* **1994**, *66* (5), 685−691.
(26) Dziewatkoski, M. P.; Daniels, L. B.; Olesik, J. W. *Anal. Chem.* **1996**, *68* (7), 1101−1109.
(27) Aeschliman, D. B.; Bajic, S. J.; Baldwin, D. P.; Houk, R. S. *J. Anal. At. Spectrom.* **2003**, *18*, 1008−1014.
(28) Tanner, M.; Günther, D. *Anal. Chim. Acta* **2009**, *633* (1), 19−28.
(29) Olesik, J. W.; Gray, P. J. *J. Anal. At. Spectrom.* **2012**, *27* (7), 1143−1155.
(30) Hineman, A.; Stephan, C. *J. Anal. At. Spectrom.* **2014**, *29* (7), 1252−1257.
(31) Abad-Álvaro, I.; Peña-Vázquez, E.; Bolea, E.; Bermejo-Barrera, P.; Castillo, J. R.; Laborda, F. *Anal. Bioanal. Chem.* **2016**, *408* (19), 5089−5097.
(32) Strenge, I.; Engelhard, C. *J. Anal. At. Spectrom.* **2016**, *31* (1), 135−144.
(33) Montaño, M. D.; Majestic, B. J.; Jämting, Å. K.; Westerhoff, P.; Ranville, J. F. *Anal. Chem.* **2016**, *88* (9), 4733−4741.
(34) Bogaerts, A.; Aghaei, M. *J. Anal. At. Spectrom.* **2017**, *32* (2), 233−261.
(35) Lindner, H.; Murtazin, A.; Groh, S.; Niemax, K.; Bogaerts, A. *Anal. Chem.* **2011**, *83* (24), 9260−9266.
(36) Lindner, H.; Bogaerts, A. *Spectrochim. Acta, Part B* **2011**, *66* (6), 421−431.
(37) Aghaei, M.; Lindner, H.; Bogaerts, A. *J. Anal. At. Spectrom.* **2012**, *27* (4), 604−610.
(38) Aghaei, M.; Lindner, H.; Bogaerts, A. *Spectrochim. Acta, Part B* **2012**, *76*, 56−64.
(39) Aghaei, M.; Lindner, H.; Bogaerts, A. *J. Anal. At. Spectrom.* **2013**, *28* (9), 1485−1492.
(40) Aghaei, M.; Flamigni, L.; Lindner, H.; Gunther, D.; Bogaerts, A. *J. Anal. At. Spectrom.* **2014**, *29* (2), 249−261.
(41) Aghaei, M.; Lindner, H.; Bogaerts, A. *Anal. Chem.* **2016**, *88* (16), 8005−8018.
(42) Aghaei, M.; Bogaerts, A. *J. Anal. At. Spectrom.* **2016**, *31* (3), 631−641.
(43) Bastús, N. G.; Comenge, J.; Puntes, V. *Langmuir* **2011**, *27* (17), 11098−11105.
(44) ANSYS FLUENT 16 Documentation, Theory Guide. 2015.
(45) Ranz, W. E.; Marshall, J. W. R. *Chem. Eng. Prog.* **1952**, *48* (3), 141−146.
(46) Lide, D. R. *CRC Handbook of Chemistry and Physics*, 83rd ed.; CRC Press LLC: Boca Raton, FL, 2002.
(47) Tuoriniemi, J.; Cornelis, G.; Hassellöv, M. *J. Anal. At. Spectrom.* **2014**, *29* (4), 743−752.
(48) *Handbook of Chemistry and Physics*, 1st ed.; Weast, R. C., Ed.; CRC Press, Inc.: Boca Raton, FL, 1988.

DOI: 10.1021/acs.analchem.8b02007
Anal. Chem. 2018, 90, 10271−10278